

Invariant Neural Ordinary Differential Equations

Ilze Amanda Auzina^{*1} Çağatay Yıldız^{*23} Sara Magliacane¹⁴ Matthias Bethge²³ Efstratios Gavves¹

Abstract

Latent neural ordinary differential equations have been proven useful for learning non-linear dynamics of arbitrary sequences. In contrast with their mechanistic counterparts, the predictive accuracy of neural ODEs decreases over longer prediction horizons (Rubanova et al., 2019). To mitigate this issue, we propose disentangling *dynamic states* from *time-invariant* variables in a completely data-driven way, enabling robust neural ODE models that can generalize across different settings. We show that such variables can control the latent differential function and/or parameterize the mapping from latent variables to observations. By explicitly modeling the time-invariant variables, our framework enables the use of recent advances in representation learning. We demonstrate this by introducing a straightforward self-supervised objective that enhances the learning of these variables. The experiments on low-dimensional oscillating systems and video sequences reveal that our disentangled model achieves improved long-term predictions, when the training data involve sequence-specific factors of variation such as different rotational speeds, calligraphic styles, and friction constants.

1. Introduction

Differential equations are the *de facto* standard for learning dynamics of biological (Hirsch et al., 2012) and physical (Tenenbaum & Pollard, 1985) systems. When the observed phenomenon is deterministic, the dynamics are typically expressed in terms of ordinary differential equations (ODEs). Traditionally, ODEs have been built from a mechanistic perspective, in which states of the observed system, as well as the governing differential function and its parameters, are specified by domain experts. The recent surge of auto-differentiation tools in machine learning has enabled *black-*

box ODEs, where the differential function is defined by a neural network, e.g. Neural ODEs (Chen et al., 2018), or a Gaussian process (Heinonen et al., 2018). These approaches have proven successful in learning surrogates for unknown differential functions in a completely data-driven way. Furthermore, when used in conjunction with encoder-decoder structures, this family of models can accurately capture the dynamics from high-dimensional sequences such as videos (Park et al., 2021; Kanaa et al., 2021).

Despite their expressive power and impressive in-distribution predictive accuracy, neural ODEs often suffer from worsening performance when extrapolated over time (Rubanova et al., 2019). Moreover, in contrast to hand-crafted mechanistic models, latent variable models such as neural ODEs are non-identifiable (Wang et al., 2021). This gets even worse when the dynamics involve discontinuous jumps and additional non-linear modules such as recurrent neural nets (Rubanova et al., 2019; De Brouwer et al., 2019). An orthogonal line of work incorporates inductive biases into architectures by defining Hamiltonian (Zhong et al., 2019), Lagrangian (Lutter et al., 2019), second-order (Yildiz et al., 2019), or graph neural network based dynamics (Poli et al., 2019). However, these methods do not address the issue that often the dynamics information is convoluted with content information within the data observations.

This work aims at disentangling dynamics from static variables in the context of neural ODEs, enabling robust neural ODE models that can generalize across different settings and improve long-term predictions. More specifically, we propose to equip the latent dynamics space with *time-invariant* variables that control either the differential function or the mapping from latent variables to observations. Considering an example of bouncing objects, our approach allows us to disentangle the dynamic states (e.g. object positions and velocities) from the static parameters modulating the dynamics (e.g. object sizes and friction), as well as from the static features irrelevant to the dynamics (e.g. colors of the objects). In our experiments, we show that a disentangled representation is key to achieving better future predictions, as well as generalization across dynamics governed by different static parameters. Our contributions are as follows:

- We extend the standard latent neural ODE model by

^{*}Equal contribution ¹University of Amsterdam ²University of Tübingen ³Tübingen AI Center ⁴MIT-IBM Watson AI Lab. Correspondence to: Ilze Amanda Auzina <i.a.auzina@uva.nl>.

disentangling the physical modeling space from static, time-invariant variables. Inspired by well-established techniques (Kondor, 2008; van der Wilk et al., 2018), we obtain time-invariant representations by averaging over the embeddings of individual time points or subsequences (Section 3.1).

- Our framework paves the way to use the recent advances in deep representation learning (Bengio et al., 2013) for dynamic modeling. To demonstrate this, we introduce a simple contrastive objective based on self-supervised representation learning (Grill et al., 2020) (Section 3.3).
- Our model consistently leads to more accurate long-term predictions as empirically shown on simulated sequences (Sections 5.1 and 5.2), rotating images (Section 5.3), and bouncing ball image sequences (Section 5.4).

While introduced for latent neural ODEs, discrete and/or stochastic dynamical systems can also benefit from the same construction. We discuss the implications of our method on learning object-centric representations and its potential Bayesian extensions (Section 6). Our implementation will be made available in GitHub upon acceptance.

2. Background

2.1. Ordinary differential equations

Multivariate ordinary differential equations are defined as

$$\dot{\mathbf{x}}(t) := \frac{d\mathbf{x}(t)}{dt} = \mathbf{f}(t, \mathbf{x}(t)), \quad (1)$$

where $t \in \mathbb{R}_+$ denotes *time*, the vector $\mathbf{x}(t) \in \mathbb{R}^d$ captures the *state* of the system at time t , and $\dot{\mathbf{x}}(t) \in \mathbb{R}^d$ is the *time derivative* of the state $\mathbf{x}(t)$. In this work, we focus on ODE systems that do not explicitly depend on time, implying a vector-valued (*time*) *differential function* $\mathbf{f} : \mathbb{R}^d \mapsto \mathbb{R}^d$. The ODE state solution $\mathbf{x}(t_1)$ is computed by integrating the differential function starting from an initial value $\mathbf{x}(t_0)$:

$$\mathbf{x}(t_1) = \mathbf{x}(t_0) + \int_{t_0}^{t_1} \mathbf{f}(\mathbf{x}(\tau)) d\tau. \quad (2)$$

Due to the deterministic nature of the differential function, the ODE state solution $\mathbf{x}(t_1)$ is completely determined by the corresponding initial value $\mathbf{x}(t_0)$.

2.2. Latent neural ODEs

Chen et al. (2018) proposed a sequential generative model, where each observed sequence $\mathbf{y}_{1:N_t} \in \mathbb{R}^{N_t \times D}$ at given time points $t_{1:N_t}$ is mapped into a *latent trajectory* $\mathbf{x}_{1:N_t} \in \mathbb{R}^{N_t \times q_x}$ with the notation $\mathbf{x}_i \equiv \mathbf{x}(t_i)$.

The generative model relies on random initial values, their continuous-time transformation, and finally an observation mapping from latent to data space, as described below:

$$\mathbf{x}_1 \sim p(\mathbf{x}_1) \quad (3)$$

$$\mathbf{x}_i = \mathbf{x}_1 + \int_{t_1}^{t_i} \mathbf{f}_\theta(\mathbf{x}(\tau)) d\tau \quad (4)$$

$$\mathbf{y}_i \sim p_\xi(\mathbf{y}_i | \mathbf{x}_i). \quad (5)$$

Here, the time differential \mathbf{f}_θ is a neural network with parameters θ (hence the name “neural ODEs”). Similar to variational auto-encoders (Kingma & Welling, 2013; Rezende et al., 2014), the “decoding” of the observations is performed by another non-linear neural network with a suitable architecture and parameters ξ .

2.3. Contrastive self-supervised learning

Contrastive representation learning aims to learn a feature extractor, as well as a representation space, where given a prescribed notion of similarity, similar data points are embedded nearby and dissimilar points are far apart (Chopra et al., 2005). Given a data point \mathbf{x} and a pair $(\mathbf{x}^+, \mathbf{x}^-)$ of positive (similar) and negative (dissimilar) samples, contrastive learning in its most general form learns a function \mathbf{g} that minimizes

$$\min \|\mathbf{g}(\mathbf{x}) - \mathbf{g}(\mathbf{x}^+)\|_2^2 - \|\mathbf{g}(\mathbf{x}) - \mathbf{g}(\mathbf{x}^-)\|_2^2, \quad (6)$$

where the similarity is defined by the Euclidean distance. While earlier works (Chopra et al., 2005; Schroff et al., 2015) define similarity using class labels and additional side information, more recent approaches rely on data augmentation (Cubuk et al., 2018; Chen et al., 2020; Zbontar et al., 2021; Grill et al., 2020).

In our work, data points or subsequences are considered similar if they are from the same data trajectory. Furthermore, as Grill et al. (2020), our learning scheme does not utilize negative pairs nor the corresponding optimization objective. We see different time frames as different instances of the same object, so there are no true negative pairs.

3. INODE: Invariant Neural ODEs

Most physical systems involve parameters that remain constant throughout a sequence¹. Such constant parameters could govern the dynamics, such as a pendulum system with different pendulum lengths/masses, or characterize the mapping from the physical modeling space to the observation space, e.g., colors of objects following the same physical rules (Li & Mandt, 2018). The generative model of the standard latent neural ODEs does not explicitly represent the

¹We use sequence to refer to a single data trajectory generated by a differential equation.

above-mentioned static variables. NODEs learn the dynamical system by simply fitting the data (sequences), hence they do not enforce the constraint that certain parts of the latent state representation $\mathbf{x}(t)$ should remain constant. Hence, we propose to extend the generative model as follows:

$$\mathbf{c} \sim p(\mathbf{c}) \quad // \text{ content variable} \quad (7)$$

$$\mathbf{m} \sim p(\mathbf{m}) \quad // \text{ dynamics modulator} \quad (8)$$

$$\mathbf{x}_1 \sim p(\mathbf{x}_1) \quad (9)$$

$$\mathbf{x}_i = \mathbf{x}_1 + \int_{t_1}^{t_i} \mathbf{f}_\theta(\mathbf{x}(\tau); \mathbf{m}) d\tau \quad (10)$$

$$\mathbf{y}_i \sim p_\xi(\mathbf{y}_i | \mathbf{x}_i; \mathbf{c}). \quad (11)$$

We broadly refer to \mathbf{c} and \mathbf{m} as *time-invariant* variables, and thus dub our method *invariant neural ODE* (INODE). Currently, for standard latent neural ODEs there is no mechanism that would explicitly allow capturing either type of time-invariant variables. In the following, we describe how our framework, INODE, explicitly models such time-invariant variables, resulting in better extrapolation and generalization abilities.

3.1. Learning latent time-invariant variables

We consider a set of observed sequences, denoted as $\mathbf{y}_{1:N_t}^{(n)}$, where $n \in \{1, \dots, N_s\}$ is the sequence index, N_s is the total number of sequences and N_t the number of time points. Since we are interested in modeling per-sequence, time-invariant variables, a straightforward modeling approach would be learning a *global* set of variables $\mathbf{C} = \{\mathbf{c}^{(1)}, \dots, \mathbf{c}^{(N_s)}\} \in \mathbb{R}^{N_s \times q_c}$ by mean-field inference (Blei et al., 2017) (similarly for $\mathbf{m}^{(n)}$). While mean-field inference usually works well in practice, it does not specify how to obtain time-invariant variables for an unobserved sequence. As we want our method to be able to generalise to unseen dynamic parametrisations, we opt for amortized inference instead, which relies on an encoder network \mathbf{g}_ψ . Next, we discuss how to learn these time-invariant variables.

(i) Content variables In order to learn a latent content variable $\mathbf{c}^{(n)}$ that captures the time-invariant characteristics of the observed sequence, we average over the observation embeddings provided by a feature extractor $\mathbf{g}_\psi(\cdot)$ (e.g., a convolutional neural network) with parameters ψ :

$$\mathbf{c}^{(n)} = \frac{1}{N_t} \sum_{i=1}^{N_t} \mathbf{c}_i^{(n)}, \quad \text{where } \mathbf{c}_i^{(n)} = \mathbf{g}_\psi(\mathbf{y}_i^{(n)}). \quad (12)$$

By construction, $\mathbf{c}^{(n)}$ is invariant to time (or more rigorously, invariant to time-dependent effects). In turn, we map back to data space via a decoder that jointly maps from the latent dynamic state and latent content variable to the observed

space (similarly to Franceschi et al. (2020)):

$$\mathbf{y}_i^{(n)} \sim p_\xi(\mathbf{y}_i^{(n)} | [\mathbf{x}_i^{(n)}, \mathbf{c}^{(n)}]) \quad \forall i \in [1, \dots, N_t]. \quad (13)$$

Note that the same content variable $\mathbf{c}^{(n)}$ is fed as input for all observations within a sequence.

(ii) Dynamics modulators Unlike content variables, dynamics modulators cannot be inferred from individual time frames as such variables manifest themselves over time. Therefore, we propose to extract these latent variables from multiple subsequent time frames of a sequence (i.e., a subsequence) instead of individual observations. Accordingly, the averaging now is over all subsequences of length N_e :

$$\mathbf{m}^{(n)} = \frac{1}{N_t - N_e} \sum_{i=1}^{N_t - N_e} \mathbf{m}_i^{(n)}, \quad \mathbf{m}_i^{(n)} = \mathbf{g}_\psi(\mathbf{y}_{i:i+N_e}^{(n)}), \quad (14)$$

where N_e is the number of subsequent observation in a subsequence and \mathbf{g}_ψ is a feature extractor with parameters ψ .

In practice, the differential function takes as input the concatenation of the dynamic state, $\mathbf{x}^{(n)}(\tau) \in \mathbb{R}^{q_x}$, and the dynamics modulator, $\mathbf{m}^{(n)} \in \mathbb{R}^{q_c}$. Therefore, we redefine the input space of the differential function: $\mathbf{f} : \mathbb{R}^{q_x + q_c} \mapsto \mathbb{R}^{q_x}$. The resulting ODE system resembles augmented neural ODEs (ANODEs) (Dupont et al., 2019), except that the augmented variables of our interest $\mathbf{m}^{(n)}$ are constant across time. It is important to note that N_e should be sufficiently big, so that the subsequences $\mathbf{y}_{i:i+N_e}^{(n)}$ would be informative about the parameter. For instance, it must hold that $N_e \geq 3$ if \mathbf{m} impacts the acceleration, which is the second-order derivative of position.

3.2. Optimization objective

The marginal likelihood $p(Y)$ for a dataset $Y \equiv \{\mathbf{y}_{1:N_t}^{(1)}, \dots, \mathbf{y}_{1:N_t}^{(N_s)}\} \in \mathbb{R}^{N_s \times N_t \times D}$ is analytically intractable due to the non-linear differential function and the decoder network. Therefore, we resort to variational inference, a common practice for neural ODE models (Chen et al., 2018; Rubanova et al., 2019)). We approximate the unknown latent initial states $\mathbf{x}_1^{(n)}$ by amortized inference:

$$\mathbf{x}_1^{(n)} \sim q_\nu(\mathbf{x}_1^{(n)} | \mathbf{y}_{1:N}), \quad (15)$$

where $q_\nu(\cdot)$ stands for an *encoding* distribution with parameters ν , which we choose to be a Gaussian with diagonal covariance. For simplicity, we chose to maintain point estimates on the content variables $\mathbf{c}^{(n)}$. The maximization objective of INODE then becomes a lower-bound (ELBO)

of the marginal likelihood (Blei et al., 2017):

$$\log p(Y) \geq \text{ELBO} = \sum_n \mathbb{E}_{q_\nu} \left[\log p(\mathbf{y}_{1:N_t}^{(n)} | \mathbf{x}_{1:N}^{(n)}) \right] - \text{KL} \left[q_\nu(\mathbf{x}_1^{(n)}) || p(\mathbf{x}_1) \right]. \quad (16)$$

We set the prior distribution to a q_x -dimensional isotropic Gaussian where q_x is specified in the experiments. We approximate the first expectation with Monte Carlo sampling of the latent trajectories. As in variational auto-encoders, the decoder outputs the parameters of the likelihood model.

Note that the optimization w.r.t. the extractor network $\mathbf{g}_\psi(\cdot)$ is implicit. More specifically, the extractor network $\mathbf{g}_\psi(\cdot)$ is trained jointly with other modules, while maximizing the ELBO objective (Eq. 16) similarly to Franceschi et al. (2020).

3.3. SINODE : Self-supervised learning of invariant variables

So far our framework does not prescribe an explicit training objective for the time-invariant variables. Yet, we could exploit the fact that the content variables $\mathbf{c}_i^{(n)}, \mathbf{c}_j^{(n)}$ of two different time points $t_i \neq t_j$ from the same n 'th data trajectory should match due to the definition of time-invariance. Inspired by the recent advances in the self-supervised learning (SSL) literature (Grill et al., 2020), we propose an SSL objective that aims to maximize the cosine similarity between *positive pairs*² of content variables

$$\max \mathcal{L}_c = \sum_{n,i,j} \frac{\mathbf{c}_i^{(n)\top} \mathbf{c}_j^{(n)}}{\|\mathbf{c}_i^{(n)}\| \|\mathbf{c}_j^{(n)}\|} \quad (17)$$

A similar objective can be also used for the dynamics modulators $\mathbf{m}^{(n)}$. More specifically, the above learning objective is equivalent to computing the cosine of an angle between two vectors. Therefore, when maximised, the objective enforces the vectors to point in the same direction, or in other words for the time-invariant variables to be similar. The benefit of this additional loss term is to prevent *temporal information leaking* into the time-invariant variables. We empirically found out that minimizing the similarity between *negative pairs* (content variables that belong to different sequences) deteriorates the overall performance. This can be explained by the observation that the sequences are not different enough for the negative pairs to exist. For example, the sequences share the underlying differential function, where the dynamics varies due to the parametrisation, hence there are no *true* negative pairs. Fig. 1 provides an example of the content variable embeddings $\{\mathbf{c}_i^{(n)}\}_{i,n=1,1}^{N_t, N_s}$, where

²We call *positive pairs* the content variables computed from the same sequence.

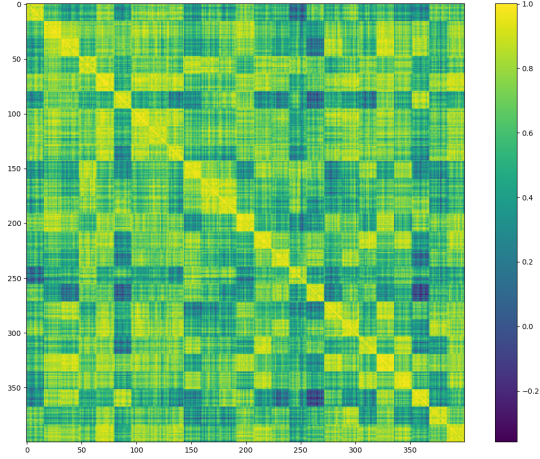


Figure 1. The cosine similarity between the content variables obtained from $N_s = 25$ data sequences with a fixed sequence length $N_t = 16$. Since each observation is mapped to a unique content variable, we obtain $N_s \times N_s = 400$ embeddings (hence, the matrix is 400×400). As indicated by the 16×16 block-matrix structure along the diagonal, the content variables $\mathbf{c}_i^{(n)}$ and $\mathbf{c}_j^{(n)}$ that belong to the same sequence have higher similarity (lighter colors) compared to pairs $\mathbf{c}_i^{(n)}$ and $\mathbf{c}_j^{(n)}$ that belong to different sequences.

each 16×16 block depicts the content variable similarity within a sequence and the goal of the proposed loss term is to maximise this value (a higher similarity).

Finally, we adjust our optimization object from section 3.2 with the SSL objective (eq.17) and maximize it with respect to all parameters:

$$\arg \max_{\theta, \nu, \psi, \xi} \text{ELBO} + \lambda \mathcal{L}_c, \quad (18)$$

where λ is a weighting term to account for the different scales of the ELBO and \mathcal{L}_c terms. We empirically validate that the model is robust to λ ; hence, for experiments with SSL objective we set $\lambda = 1$ and call the resulting model SINODE.

4. Related work

Neural ODEs Since the neural ODE breakthrough (Chen et al., 2018), there has been a growing interest in continuous-time dynamics modeling. Such attempts include combining recurrent neural nets with neural ODE dynamics (Rubanova et al., 2019; De Brouwer et al., 2019) where latent trajectories are updated upon observations, as well as Hamiltonian (Zhong et al., 2019), Lagrangian (Lutter et al., 2019), second-order (Yildiz et al., 2019), or graph neural network based dynamics (Poli et al., 2019). While our method IN-ODE (as well as the extension SINODE) has been introduced in the context of latent neural ODEs, it can be directly

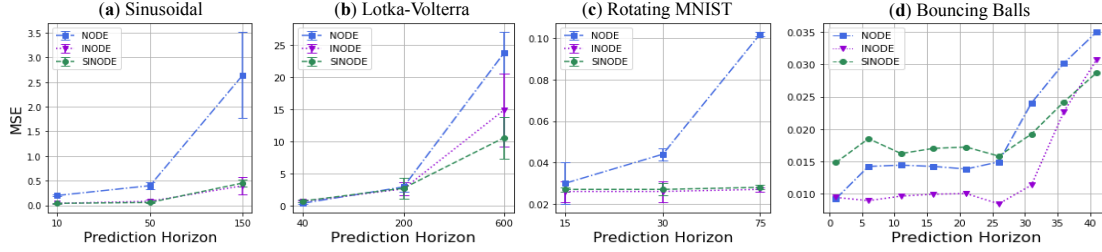


Figure 2. Test MSE across different datasets and varying time horizons. Standard deviation of test MSE plotted as error bars. (a-b) For sinusoidal data and Lotka-Volterra, the predictive horizon corresponds to (i) the length T_{in} of the subsequence used by the models to extract latent variables, (ii) the length N_t of training sequences and (iii) a bigger forecasting range ($3N_t$). (c) For rotating MNIST, the MSE is measured at times N_t , $2N_t$, and $5N_t$. (d) For bouncing ball, the MSE is computed against an increasing length of prediction horizon, noting $N_t = 25$.

utilized within these frameworks as well.

Augmented dynamics Dupont et al. (2019) augment data-space neural ODEs with additional latent variables and test their method only on classification problems. Norcliffe et al. (2021) extend neural ODEs to stochastic processes by means of a stochastic, latent variable modulating the dynamics. In a related study, Yildiz et al. (2022) propose to infer latent variables modulating data-space for Gaussian process based ODEs, with applications to low-dimensional problems. To the best of our knowledge, we are the first to explicitly enforce time-invariant variables.

Disentanglement and learning invariances Our learning scheme for time-invariant variables is closest to Grill et al. (2020) in that neither formulation involves negative pairs. The idea of averaging for invariant function estimation was used in (Kondor, 2008; van der Wilk et al., 2018; Franceschi et al., 2020). The latter proposes using such variables in the context of discrete-time stochastic video prediction. Although relevant, their model involves two sets of dynamic latent variables, coupled with an LSTM.

5. Experiments

Datasets We benchmark on four different datasets with varying complexity of the dynamics, as well as data dimensionality: sinusoidal dataset (Section 5.1), Lotka-Volterra dataset (Section 5.2), Rotating MNIST Casale et al. (2018), Section 5.3, and bouncing balls (Sutskever et al. (2008), Section 5.4). For the details of the datasets, please see App. A.

Implementation details We implement our model in PyTorch (Paszke et al., 2017). The encoder, decoder, differential function, and invariant encoder network are all jointly optimized with the Adam optimizer (Kingma & Ba, 2014) with learning rate 0.002. For solving the ODE systems we use `torchdiffeq` (Chen, 2018) package. For more

details on hyperparameters, ODE solvers and architecture details, see App. B.

Compared methods In all experiments, we compare standard neural ODE (NODE, Chen et al. (2018)) with our frameworks: (a) INODE - adding time-invariant variables, and (b) SINODE - adding time-invariant variables and an additional SSL training objective. We use the same network architectures for all compared models to isolate the effects of time-invariant representation and SSL objective. We do not compare against augmented neural ODEs (Dupont et al., 2019), as they present their methodology in the context of density estimation and classification. Furthermore, the predictions of another similar work by Norcliffe et al. (2021) have fallen back to the prior; hence, we did not include any results in this version.

Comparison goals In all experiments, we aim to demonstrate whether time-invariant variables improve (i) generalization to new test sequences that follow different content variables \mathbf{c} and dynamics modulators \mathbf{m} , and (ii) extrapolation to longer time horizons. In particular, the sinusoidal, Lotka-Volterra, and bouncing balls datasets are used to confirm the utility of *dynamics modulators*, while the rotating MNIST dataset is used to verify the advantage of the *content variables*.

Note that during training, all models use the first T_{in} observations as input to encode the latent initial states $\mathbf{x}_0^{(n)}$. In addition, our framework uses T_{inv} observations to extract the time-invariant variables \mathbf{c} and \mathbf{m} . For a fair comparison with NODE, we ensure that all models use the same number of data points to extract latent variables, and also the latent dimensionalities match. We test the extrapolation performance by comparing the mean squared errors (MSE) over time horizons that exceed the training length N_t .

Reported metrics In order to evaluate the performance of our framework, we report the test MSE at different sequence lengths (time-horizons), empirically compare the

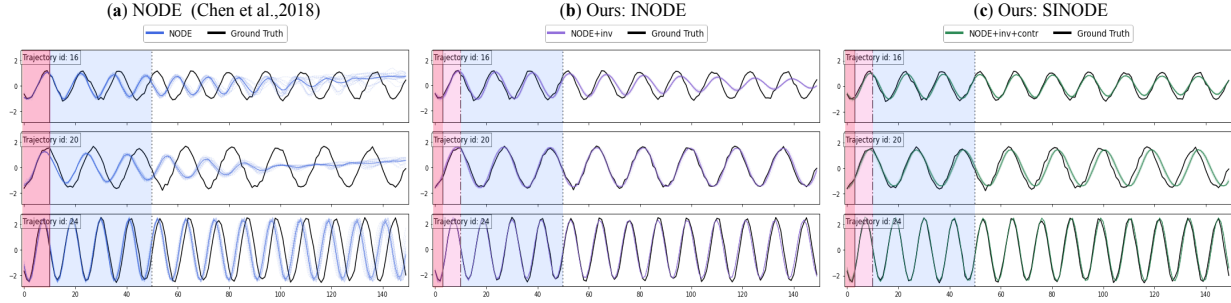


Figure 3. Model forecasting accuracy on test sinusoidal sequences. (a) NODE Chen et al. (2018); (b) INODE (ours); (c) SINODE (ours). The black curve is the ground truth, the thick colored curve is the mean model predictions (computed across 20 Monte Carlo samples), and the lighter curves represent the samples (for INODE and SINODE not visible as the predictions match almost perfectly across samples). At training time, the models are conditioned on the points in the red area (to extract the latent variables) and reconstruct points in the blue area. For INODE and SINODE the dynamics modulating variable is learned from points in the pink area (including the preceding red area). At test time, the models are rolled out for a longer time horizon ($N_t = 150$).

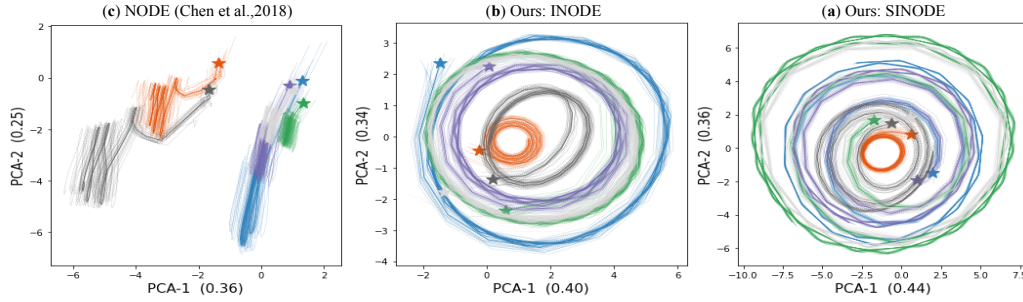


Figure 4. PCA embeddings of six latent sinusoidal trajectories. Each curve $\mathbf{x}_{1:N_t}^{(n)}$ above is obtained from a distinct data trajectory. The numbers in the axis labels denote the explained variance. Each color indicates a different sample and stars are the initial values. Each trajectory contains 150 time points. Fainted lines correspond to 20 samples from the model, while the thicker lines are the mean trajectories.

reconstructed sequences, as well as investigate the latent space learned by the models.

5.1. Sinusoidal data

We experiment with sinusoidal sequences (Rubanova et al., 2019; Norcliffe et al., 2021), where the generated sequences have different initial position, frequency, and amplitude across them (for the equations, see Eq. 22 in App. A). The empirical results are presented in Fig. 3 (for additional sequences see Fig. 12 in App. C), where we show that our framework generalizes across unseen dynamic parametrisation, as well as improves forecasting accuracy. More specifically, standard NODE model fails to extrapolate beyond the training regime, especially for sin waves with low frequency. In contrast, INODE and SINODE show consistent predictions also far in the future. The latent space trajectories plotted in Fig. 4 in App. C confirm the benefit of disentangling the dynamics modulators from the underlying dynamics. Moreover, the higher predictive accuracy of our methods is also shown in Fig. 2 (a), where our framework obtains a lower MSE than standard NODE across both

medium and long sequence lengths. Lastly, the addition of the SSL objective brings minor improvements, as seen by more consistent amplitude across different time steps in Fig. 3 and higher explained variance in Fig. 4 in App. C.

5.2. Lotka-Volterra (LV) benchmark

Next, we test our methodology on the Lotka-Volterra benchmark (Rubanova et al., 2019; Norcliffe et al., 2021), governed by a pair of first-order nonlinear differential equations describing the predator-prey dynamics (Eq. 27 in App. A). The generated trajectories have different initial positions and parameters that describe the interaction between the two populations across data sequences. Similar to sinusoidal data, the time-invariant variable of interest is the one that governs the dynamics, i.e. the interaction parameters.

The empirical results confirm the initial observations gained from the sinusoidal dataset: *dynamics modulators* improve the predictive abilities of a NODE model for a dynamical system, as seen in Fig. 15 in App. C. In particular, even though NODE fits the training sequences well ($N_t = 200$)

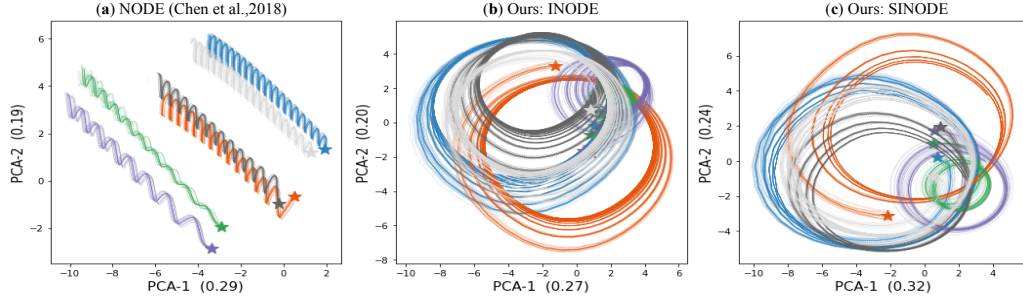


Figure 5. PCA embeddings of six latent Lotka-Volterra trajectories, each with a different color. In total six samples are plotted for a horizon of 200. We argue that the true underlying two-dimensional dynamics are better captured by our INODE and SINODE.

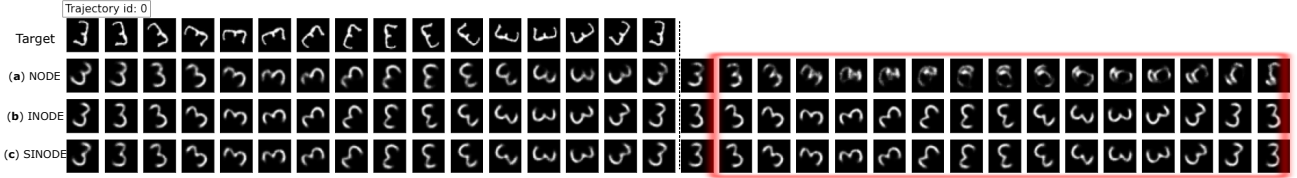


Figure 6. Model predictions on a rotating MNIST test sequence. (a) NODE Chen et al. (2018) (b) INODE (ours). (c) SINODE (ours). At training time, NODE is conditioned on $T_{in} = 5$, while INODE and SINODE condition on $T_{in} = 1$. Reconstructions are performed for $N_t = 16$. The time-invariant content variable is learned from $T_{inv} = 16$ time frames. At test time, we roll out the model for a longer prediction horizon ($N_t = 30$). The red colored box indicates where our model succeeds, but standard NODE fails.

outside this training regime the performance of the model drops massively, while our INODE, SINODE circumvent this. The test MSE confirms the empirical observations, see Fig. 2 (b). For sequences $< T_N$, the performance of NODE is on par with our framework (see Fig. 14 in App. C), but on longer sequences our approach is superior as indicated by a lower MSE.

Furthermore, we also visualise the generated latent space of the test sequences in Fig. 5. The latent plots of our framework are more aligned with the true dynamics as they better match the commonly observed phase diagrams of LV dynamics (see Fig. 14 in App. C). Lastly, the addition of the SSL loss term brings minor improvements. In particular, it is beneficial when the frequency of the observation is low, see Fig. 15 in App. C. In such cases, when the data is limited, having an additional constraint might be beneficial for the model.

5.3. Rotating MNIST

We show that time-invariant variables are also useful for high-dimensional data, e.g. video sequences, by generating a dataset of rotating images of handwritten “3” digits taken from the MNIST dataset (LeCun, 1998). We consider the same number of rotation angles ($N_t = 16$) as Casale et al. (2018); Solin et al. (2021). We randomize the initial rotational angle, but the rotation speed is kept fixed across all sequences. In this set-up the content variable is the style of the digit. Hence, it does not affect the underlying dynamics.

The empirical results in Fig. 6 confirm that our framework is beneficial for learning dynamics also from high-dimensional data sequences (for more sequences see Fig. 17 in App. C). The reconstruction quality is good across all models within the sequence length seen during training ($N_t = 16$). However, already within a single forward pass NODE model fails to reconstruct the true digit (see the red frame in Fig. 6), while INODE and SINODE not only reconstruct the original style of the digit, but also capture the correct frequency of the periodic movement.

The test MSE scores align with this observation. Our framework outperforms NODE with increasing sequence length, see Fig. 2 (c). The latent plots of the test trajectories explain why NODE fails on longer sequences (Fig. 18 in App. C). Even though the NODE model has learned a rotation, the latent space is noisier as the latent variable also contains information about the style of the digit, while for our framework the latent space forms almost perfect circles. Lastly, the additional SSL loss objective does not seem to bring any benefits for this use case.

As an ablation study, we test our model on the same dataset with a sequence length of $N_t = 6$ and twice the number of training sequences. This constitutes a more challenging dataset since sequences do not even form half of a loop. We replicated all the results above with MSE worsened by 30%.

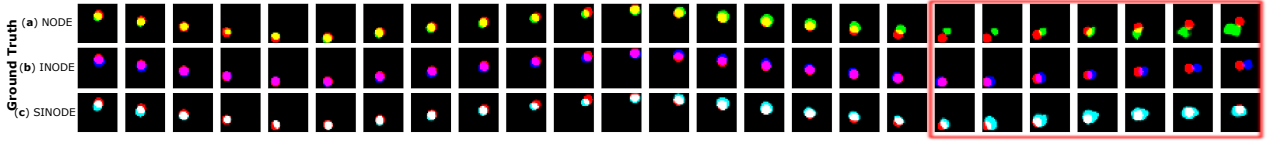


Figure 7. Bouncing ball test reconstructions for every other observation. The rows contrast the ground truth predictions (red circles) against the three models (note that the dataset is greyscaled, colors here are only used for demonstration). At training time, NODE and INODE, SINODE condition on $T_{in} = 10$. The time-invariant content variable is learned from $T_{inv} = 10$ time frames. At test time, we roll out the model for a larger time interval ($N_t = 50$). The red colored box indicates where discrepancy across model can be observed.

5.4. Bouncing ball with friction

To investigate our model’s performance on video sequences we test it on the bouncing balls dataset, a benchmark often used in temporal generative modeling (Sutskever et al., 2008; Gan et al., 2015; Yildiz et al., 2019). For data generation, we modify the original implementation of Sutskever et al. (2008) by adding friction to the system. We assume a per-sequence friction constant, which slows down the ball by a constant factor.

Our framework improves predictive capability for video sequences as confirmed by empirical observations, see Fig. 7 (for additional sequences see Fig. 19 in App. C) and test MSE (Fig. 2 (c)). More specifically, standard NODE model fails to predict the correct position of the object at further time horizons, while our framework INODE corrects this error (see Fig. 7 red box). Furthermore, the dynamics modulating variable is beneficial even at short prediction horizons, as visible in Fig. 2 (c). Nonetheless, the addition of the SSL loss term does not bring any benefits.

5.5. Ablation studies

Lastly, we perform ablation studies on Lotka-Volterra dataset. In particular, we demonstrate the effect of (i) the number N_s of training sequences, (ii) the length T_{in} of the subsequence from which the models extract latent variables, (iii) the numerical ODE solver, (iv) the dimensionality q_x, q_c of the latent dynamic and time-invariant variables, and (v) the loss weighting term λ . We repeat each experiment 4 times, and report the mean and standard deviation across repetitions. Here we summarize the main findings and refer to Table 2 in the Appendix for further details. First, we observe that the error decreases with more training sequences and longer inputs from which latent variables are extracted. Next, the fixed-step ODE solvers (Euler and RK4) give slightly better results than an adaptive-step solver (dopri5). The model seems to be somewhat robust to the latent dimensionality, while very small/large values impair learning as usual. Finally, we observe that a moderate value for the self-supervised learning weight λ leads to a better MSE than having very strong or no self-supervision. Although the variance of the results makes comparisons dif-

ficult, the results indicate that λ should be carefully chosen with cross-validation.

6. Discussion

We have presented an extension to NODE models for invariant dynamical modeling. We introduce a time-invariant variable $c^{(n)}$ that can model the content of the observed system and time-invariant variables $m^{(n)}$ that can modulate the dynamics, resulting in an INODE model. Furthermore, we investigate an additional constraint on these time-invariant variables via a self-supervised loss (17) that enforces similarity across time points, hence we call the subsequent model SINODE. Our empirical results confirm that our framework leads to more accurate long-term predictions on simulated and video sequences, is able to generalise to new dynamic parametrisations and, as such, improves the existing continuous latent space models.

The main focus of the presented work is on deterministic periodic systems. This could be extended to stochastic dynamics via an auxiliary variable that models the noise, similarly to Franceschi et al. (2020). Furthermore, our framework can easily be used also in other temporal models. Specifically, it could be combined with a Gaussian process-based ODEs (Hegde et al., 2022), leading to a Bayesian extension to the present framework. Likewise, time invariances can be inferred via marginal likelihood as in (van der Wilk et al., 2018; Schwöbel et al., 2022), which would lead to a more holistic Bayesian framework. Lastly, our framework could be extended to object-centric dynamical modeling, which would learn per-object representations coupled with a single dynamical model.

References

- Bengio, Y., Courville, A., and Vincent, P. Representation learning: A review and new perspectives. *IEEE transactions on pattern analysis and machine intelligence*, 35(8): 1798–1828, 2013.
- Blei, D. M., Kucukelbir, A., and McAuliffe, J. D. Variational inference: A review for statisticians. *Journal of the American statistical Association*, 2017.

- Casale, F. P., Dalca, A., Saglietti, L., Listgarten, J., and Fusi, N. Gaussian process prior variational autoencoders. *Advances in neural information processing systems*, 31, 2018.
- Chen, R. T., Rubanova, Y., Bettencourt, J., and Duvenaud, D. K. Neural ordinary differential equations. *Advances in neural information processing systems*, 31, 2018.
- Chen, R. T. Q. torchdiffeq, 2018. URL <https://github.com/rtqichen/torchdiffeq>.
- Chen, T., Kornblith, S., Norouzi, M., and Hinton, G. A simple framework for contrastive learning of visual representations. In *International conference on machine learning*, pp. 1597–1607. PMLR, 2020.
- Chopra, S., Hadsell, R., and LeCun, Y. Learning a similarity metric discriminatively, with application to face verification. In *2005 IEEE Computer Society Conference on Computer Vision and Pattern Recognition (CVPR’05)*, volume 1, pp. 539–546. IEEE, 2005.
- Cubuk, E. D., Zoph, B., Mane, D., Vasudevan, V., and Le, Q. V. Autoaugment: Learning augmentation policies from data. *arXiv preprint arXiv:1805.09501*, 2018.
- De Brouwer, E., Simm, J., Arany, A., and Moreau, Y. Gru-ode-bayes: Continuous modeling of sporadically-observed time series. *Advances in neural information processing systems*, 32, 2019.
- Dupont, E., Doucet, A., and Teh, Y. W. Augmented neural ODEs. In *Advances in Neural Information Processing Systems*, 2019.
- Franceschi, J.-Y., Delasalles, E., Chen, M., Lamprier, S., and Gallinari, P. Stochastic latent residual video prediction. In *International Conference on Machine Learning*, pp. 3233–3246. PMLR, 2020.
- Gan, Z., Li, C., Henao, R., Carlson, D. E., and Carin, L. Deep temporal sigmoid belief networks for sequence modeling. *Advances in Neural Information Processing Systems*, 28, 2015.
- Grill, J.-B., Strub, F., Altché, F., Tallec, C., Richemond, P., Buchatskaya, E., Doersch, C., Avila Pires, B., Guo, Z., Gheshlaghi Azar, M., et al. Bootstrap your own latent-a new approach to self-supervised learning. *Advances in neural information processing systems*, 33:21271–21284, 2020.
- Hegde, P., Yıldız, Ç., Lähdesmäki, H., Kaski, S., and Heinonen, M. Variational multiple shooting for bayesian odes with gaussian processes. In *Uncertainty in Artificial Intelligence*, pp. 790–799. PMLR, 2022.
- Heinonen, M., Yıldız, C., Mannerström, H., Intosalmi, J., and Lähdesmäki, H. Learning unknown ode models with gaussian processes. In *International Conference on Machine Learning*, pp. 1959–1968. PMLR, 2018.
- Hirsch, M. W., Smale, S., and Devaney, R. L. *Differential equations, dynamical systems, and an introduction to chaos*. Academic press, 2012.
- Kanaa, D., Voleti, V., Kahou, S. E., and Pal, C. Simple video generation using neural odes. *arXiv preprint arXiv:2109.03292*, 2021.
- Kingma, D. P. and Ba, J. Adam: A method for stochastic optimization. *arXiv preprint arXiv:1412.6980*, 2014.
- Kingma, D. P. and Welling, M. Auto-encoding variational bayes. *arXiv preprint arXiv:1312.6114*, 2013.
- Kondor, I. R. *Group theoretical methods in machine learning*. Columbia University, 2008.
- LeCun, Y. The mnist database of handwritten digits. <http://yann.lecun.com/exdb/mnist/>, 1998.
- Li, Y. and Mandt, S. Disentangled sequential autoencoder. *arXiv preprint arXiv:1803.02991*, 2018.
- Lutter, M., Ritter, C., and Peters, J. Deep lagrangian networks: Using physics as model prior for deep learning. *arXiv preprint arXiv:1907.04490*, 2019.
- Norcliffe, A., Bodnar, C., Day, B., Moss, J., and Liò, P. Neural ode processes. *ICLR*, 2021.
- Park, S., Kim, K., Lee, J., Choo, J., Lee, J., Kim, S., and Choi, E. Vid-ode: Continuous-time video generation with neural ordinary differential equation. In *Proceedings of the AAAI Conference on Artificial Intelligence*, volume 35, pp. 2412–2422, 2021.
- Paszke, A., Gross, S., Chintala, S., Chanan, G., Yang, E., DeVito, Z., Lin, Z., Desmaison, A., Antiga, L., and Lerer, A. Automatic differentiation in pytorch. 2017.
- Poli, M., Massaroli, S., Park, J., Yamashita, A., Asama, H., and Park, J. Graph neural ordinary differential equations. *arXiv preprint arXiv:1911.07532*, 2019.
- Rezende, D. J., Mohamed, S., and Wierstra, D. Stochastic backpropagation and approximate inference in deep generative models. In *International conference on machine learning*, pp. 1278–1286. PMLR, 2014.
- Rubanova, Y., Chen, R. T., and Duvenaud, D. K. Latent ordinary differential equations for irregularly-sampled time series. *Advances in neural information processing systems*, 32, 2019.

- Schroff, F., Kalenichenko, D., and Philbin, J. Facenet: A unified embedding for face recognition and clustering. In *Proceedings of the IEEE conference on computer vision and pattern recognition*, pp. 815–823, 2015.
- Schwöbel, P., Jørgensen, M., Ober, S. W., and Van Der Wilk, M. Last layer marginal likelihood for invariance learning. In *International Conference on Artificial Intelligence and Statistics*, pp. 3542–3555. PMLR, 2022.
- Solin, A., Tamir, E., and Verma, P. Scalable inference in sdes by direct matching of the fokker–planck–kolmogorov equation. *Advances in Neural Information Processing Systems*, 34:417–429, 2021.
- Sutskever, I., Hinton, G. E., and Taylor, G. W. The recurrent temporal restricted boltzmann machine. *Advances in neural information processing systems*, 21, 2008.
- Tenenbaum, M. and Pollard, H. *Ordinary differential equations: an elementary textbook for students of mathematics, engineering, and the sciences*. Courier Corporation, 1985.
- van der Wilk, M., Bauer, M., John, S., and Hensman, J. Learning invariances using the marginal likelihood. *Advances in Neural Information Processing Systems*, 31, 2018.
- Wang, Y., Blei, D., and Cunningham, J. P. Posterior collapse and latent variable non-identifiability. *Advances in Neural Information Processing Systems*, 34:5443–5455, 2021.
- Yildiz, C., Heinonen, M., and Lahdesmaki, H. Ode2vae: Deep generative second order odes with bayesian neural networks. *Advances in Neural Information Processing Systems*, 32, 2019.
- Yıldız, Ç., Kandemir, M., and Rakitsch, B. Learning interacting dynamical systems with latent gaussian process odes. *arXiv preprint arXiv:2205.11894*, 2022.
- Zbontar, J., Jing, L., Misra, I., LeCun, Y., and Deny, S. Barlow twins: Self-supervised learning via redundancy reduction. In *International Conference on Machine Learning*, pp. 12310–12320. PMLR, 2021.
- Zhong, Y. D., Dey, B., and Chakraborty, A. Symplectic ode-net: Learning hamiltonian dynamics with control. *arXiv preprint arXiv:1909.12077*, 2019.

A. Experiment details

Below, we describe the data simulation. Please refer to Table 1 for other properties of the datasets..

Sin data In the same vein as (Rubanova et al., 2019; Norcliffe et al., 2021), we first define a set of time points $T = \{0, 0.1, 0.2, \dots, t_i, \dots, 4.9\}$. Then each sequence $\mathbf{y}^{(n)}$ is generated as follows:

$$a^{(n)} \sim \mathbb{U}[1, 3] \quad (19)$$

$$f^{(n)} \sim \mathbb{U}[0.5, 1.0] \quad (20)$$

$$\phi^{(n)} \sim \mathbb{U}[0, 1.0] \quad (21)$$

$$x_i^{(n)} = a^{(n)} \sin \left(f^{(n)} t_i + \phi^{(n)} \right) \quad (22)$$

$$y_i^{(n)} \sim \mathcal{N}(x_i^{(n)}, 0.1) \quad (23)$$

where \mathbb{U} denotes the uniform distribution.

Lotka-Volterra data To generate Lotka-Volterra sequences, we follow a similar generative model as above.

$$\alpha^{(n)} \sim \mathbb{U}[.1, .4] \quad (24)$$

$$\gamma^{(n)} \sim \mathbb{U}[.1, .4] \quad (25)$$

$$\mathbf{x}_0^{(n)} \sim \mathbb{U}[2, 10] \quad (26)$$

$$\mathbf{x}_i^{(n)} = \mathbf{x}_0^{(n)} + \int_0^{t_i} \begin{bmatrix} \alpha^{(n)} x_1^{(n)}(\tau) - x_1^{(n)}(\tau) x_2^{(n)}(\tau) / 2 \\ x_1^{(n)}(\tau) x_2^{(n)}(\tau) / 5 - \gamma^{(n)} x_2^{(n)}(\tau) \end{bmatrix} d\tau \quad (27)$$

$$\mathbf{y}_i^{(n)} \sim \mathcal{N}(\mathbf{x}_i^{(n)}, 0.1) \quad (28)$$

Bouncing ball with friction For data generation, we use the script provided by Sutskever et al. (2008). As a tiny update, each observed sequence has a friction constant drawn from a uniform distribution $\mathbb{U}[0, 0.02]$. We set the initial velocities to be unit vectors with random directions.

Table 1. Details of the datasets. Below, N denotes the number of sequences (for training, validation, and test), N_t is the sequence length, Δt denotes the time between two observations, σ is the standard deviation of the added noise, T_{in} denotes the number of initial time points the initial value encoder takes as input, T_{inv} is the number of time points used to extract the invariant representations $\mathbf{c}^{(n)}$. Further, q_x and q_c denote, respectively, the dimensionality of the dynamic state $\mathbf{x}(t)$ and the invariant representation for our model variant. For a fair comparison, the latent dimensionality of the neural ODE model is always set to $q_x + q_c$.

DATASET	N_{tr}	N_{val}	N_{test}	N_t	Δt	σ	T_{in} (NODE)	T_{in}	T_{inv}	q_x	q_c
SINUSOIDAL DATA	80	25	25	50	0.1	0.1	10	3	10	4	4
LOTKA-VOLTERRA	500	100	100	200	0.1	0.1	40	8	40	8	8
ROTATING MNINST	500	60	60	16	0.1	0.0	5	1	16	10	16
BOUNCING BALL WITH FRICTION	2000	100	100	25	1.0	0	10	10	10	10	2

Table 2. Ablation studies performed on Lotka-Volterra dataset. We repeat each experiment 4 times, and report the mean and standard deviation across repetitions. In each table, we vary one factor and compare the results against the standard setup marked by \star in each table ($N_{tr} = 500$, $T_{inv} = 40$, SOLVER = EULER, $q_x = 8$, $q_c = 8$, $\lambda = 1.0$). **(a-b)** As expected, the error decreases with more data points and input to which the predictions are conditioned on. **(c)** dopri5 solver leads to slightly worse predictions than fixed step solvers Euler and RK4. **(d)** The model seems to be somewhat robust to the dimensionality of the dynamic states q_x and time-invariant representations q_c . **(e)** Finally, we observe that a moderate value for the self-supervised learning weight λ leads to a better MSE than having very strong or no self-supervision. Although the variance of the results makes comparisons difficult, the results indicate that λ should be carefully chosen with cross-validation.

(a)		(b)		(c)	
N_{tr}	MSE	T_{inv}	MSE	ODE SOLVER	MSE
100	9.750 ± 1.296	10	5.283 ± 1.344	EULER*	3.643 ± 0.406
250	4.999 ± 0.671	20	4.490 ± 0.562	RK4	3.646 ± 0.777
500*	3.643 ± 0.406	40*	3.643 ± 0.406	DOPRI5	4.147 ± 0.391
		80	2.412 ± 0.177		

(d)			(e)	
q_x	q_c	MSE	λ	MSE
2	2	4.617 ± 1.632	0	3.452 ± 0.182
2	8	3.818 ± 0.679	1.0*	3.643 ± 0.406
8	2	3.503 ± 0.389	10.0	3.103 ± 0.457
4	4	3.762 ± 0.262	100.0	3.665 ± 0.322
8*	8*	3.643 ± 0.406	1000.0	4.405 ± 0.338
16	16	3.915 ± 0.601		

B. Architecture and Hyperparameter Details

Table 3. Brief overview of the model architecture per dataset. Overall, the architecture of our model consists of 4 main parts: (a) Position Encoder; (b) Invariant Encoder; (c) Differential Function; and (d) Decoder.

DATASET	Position Encoder	Invariant Encoder	Differential Function	Solver (dt)	Decoder
SINUSOIDAL DATA	RNN	RNN	MLP	euler (0.1)	MLP
LOTKA-VOLTERRA	RNN	RNN	MLP	euler (0.1)	MLP
ROTATING MNINST	CNN	CNN	MLP	dopri5 (0.1)	CNN
BOUNCING BALL WITH FRICTION	CNN	RNN	MLP	dopri5 (0.1)	CNN

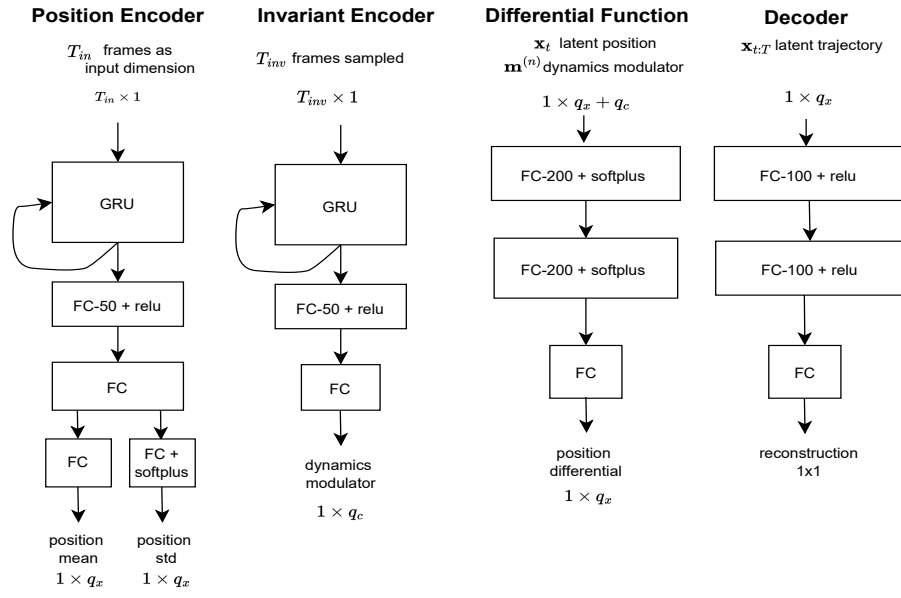


Figure 8. INODE or SINODE architecture for Sinusoidal data. For NODE architecture is similar, but without the 'Invariant Encoder'.

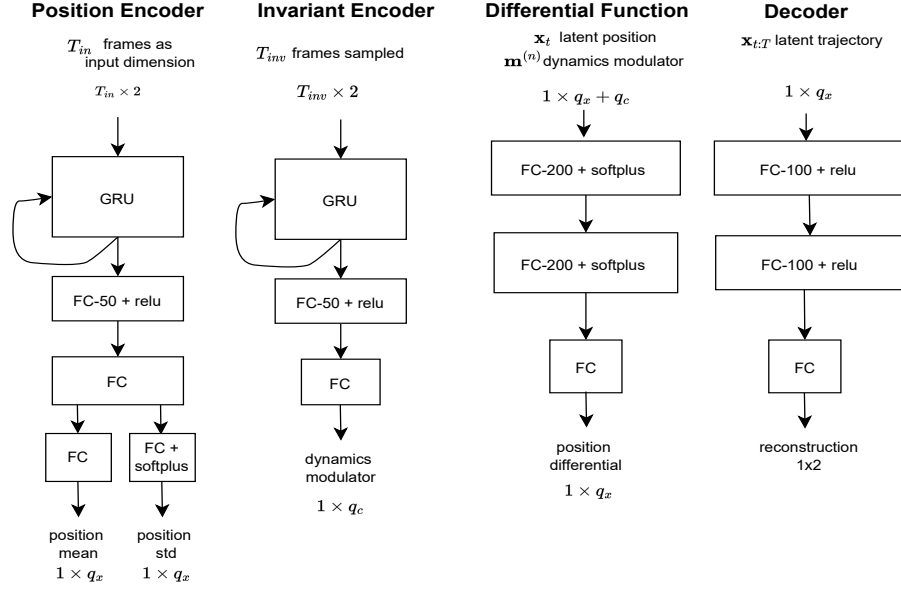


Figure 9. INODE or SINODE architecture for Lotka-Volterra data. For NODE architecture is similar, but without the 'Invariant Encoder'.

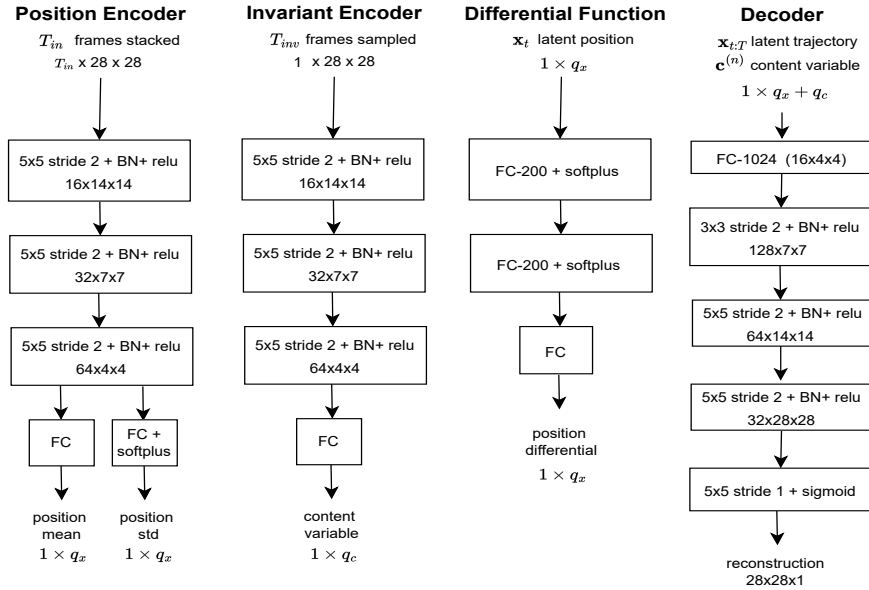


Figure 10. INODE or SINODE architecture for Rotating MNIST. For NODE architecture is similar, but without the 'Invariant Encoder'.

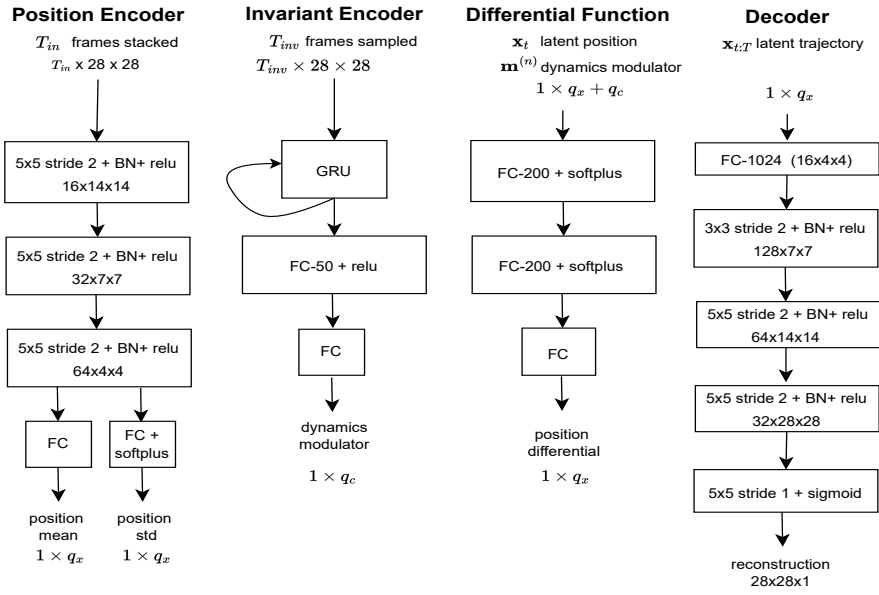


Figure 11. INODE or SINODE architecture for Bouncing Balls. For NODE architecture is similar, but without the 'Invariant Encoder'.

C. Additional Results

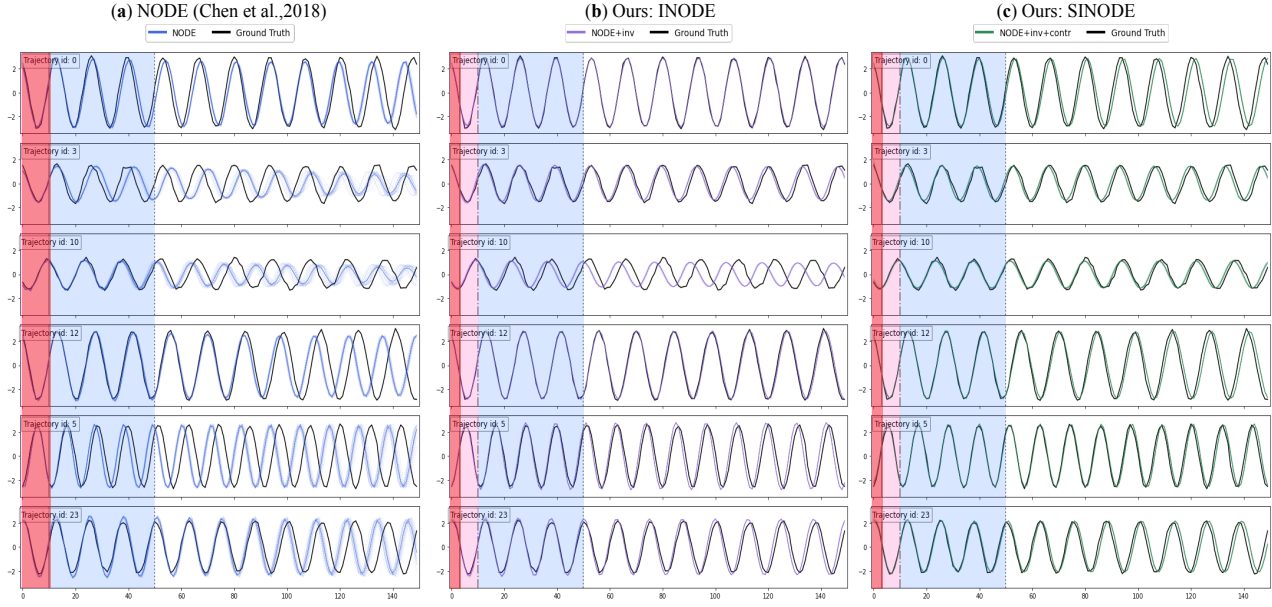


Figure 12. Model forecasting accuracy on test sinusoidal sequences. (a) NODE [Chen et al. \(2018\)](#); (b) INODE (ours); (c) SINODE (ours). The black line is the ground truth, thick colored line is the mean across 20 samples, while lighter lines represent each sample (for INODE and SINODE not visible as the predictions match almost perfectly across samples). At training time, the model conditions on points in the red area and reconstructs points in the blue area. For INODE and SINODE the dynamics modulating variable is learned from points in the pink area (including the the proceeding red area). At test time, the model is rolled out for a longer time interval ($N_t = 150$).

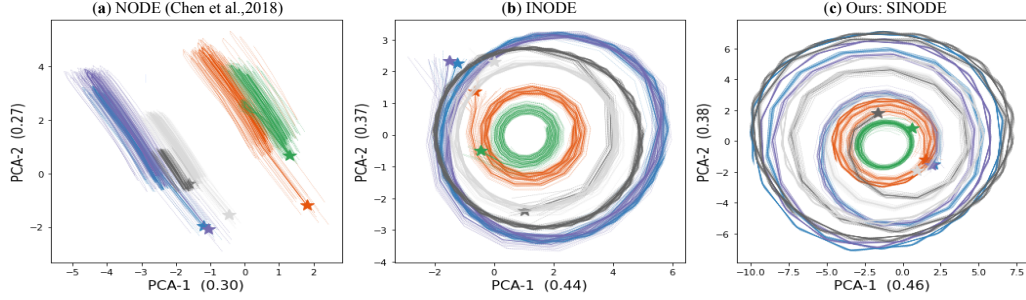


Figure 13. Sampled sinusoidal sequence latent space. (a) NODE as in [Chen et al. \(2018\)](#). (b) INODE (ours). (c) SINODE (ours). A star indicates the beginning of a trajectory, while color indicates a data sample. In total six samples are plotted for $N_t=150$. Fainted lines correspond to samples from the model, in total 20, while the thicker line is the mean value.

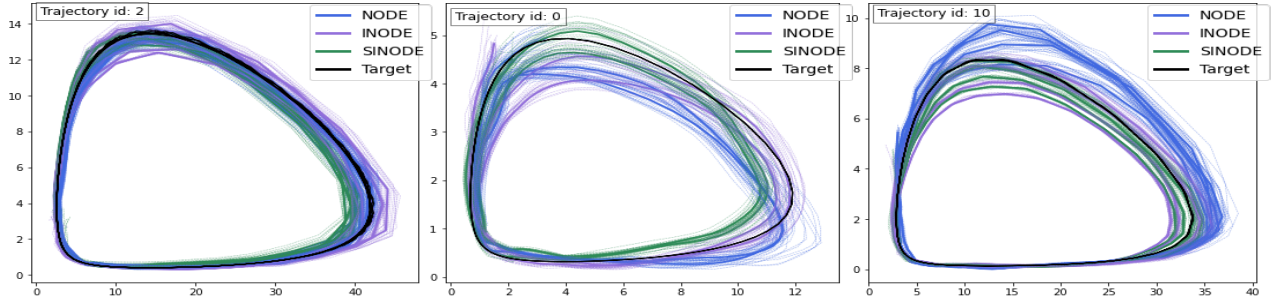


Figure 14. Lotka-Volterra Phase Diagram. Black line indicates the underlying ground truth; green: SINODE; purple: INODE; blue: NODE (Chen et al., 2018). Dashed lines correspond to samples from the corresponding model ($L=20$), while thicker colored line is the mean

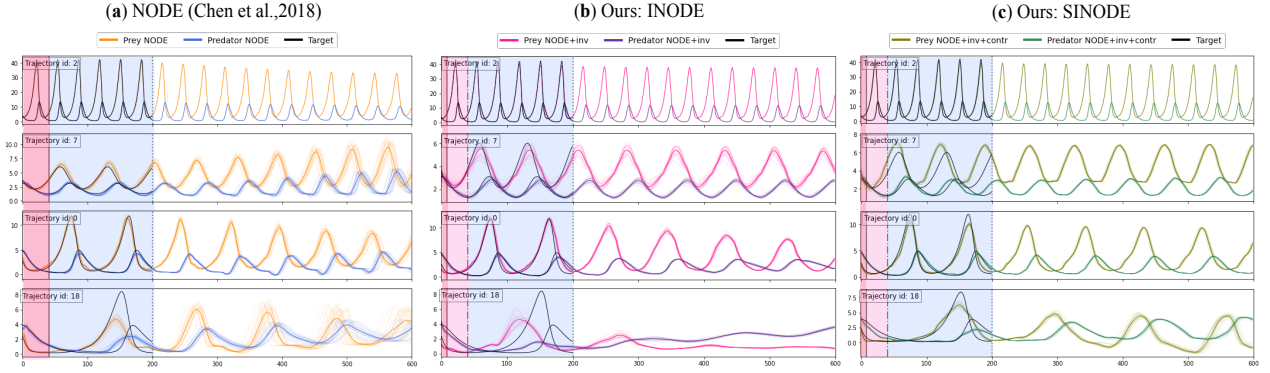


Figure 15. Model forecasting accuarcy on test Lotka-Volterra sequences. (a) NODE Chen et al. (2018); (b) INODE (ours); (c) SINODE (ours). The black line is the ground truth, thick colored line is the mean across 20 samples, while lighter lines represent each sample (for INODE and SINODE not visible as the predictions match almost perfectly across samples). At training time, the model conditions on points in the red area, and reconstructs points in the blue area. For INODE and SINODE the dynamics modulating variable is learned from points in the pink area (including the the proceeding red area). At test time, the model is rolled out for a longer time interval ($N_t = 600$).

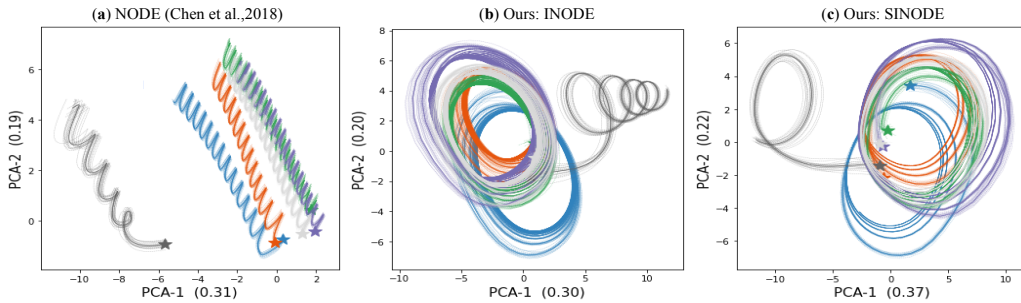


Figure 16. Sampled LV sequence latent space. (a) NODE Chen et al. (2018). (b) INODE(ours). (c) SIONDE (ours). A star indicates the beginning of a trajectory, while color indicates a data sample. In total six samples are plotted for $N_t=200$. Fainted lines correspond to samples from the model, in total 20, while the thicker line is the mean value.



Figure 17. Model prediction accuracy on test Rotating MNIST trajectories. (a) NODE [Chen et al. \(2018\)](#) (b) INODE (ours). (c) SINODE (ours). At training time, NODE conditions on $T_{in} = 5$, while INODE and SINODE condition on $T_{in} = 1$. Reconstructs are performed for $N_t = 16$. Time-invariant content variable is learned from $T_{inv} = 16$ time frames. At test time, we roll out the model for a larger time interval ($N_t = 30$). The red colored box indicates where our model succeeds but standard NODE fails.

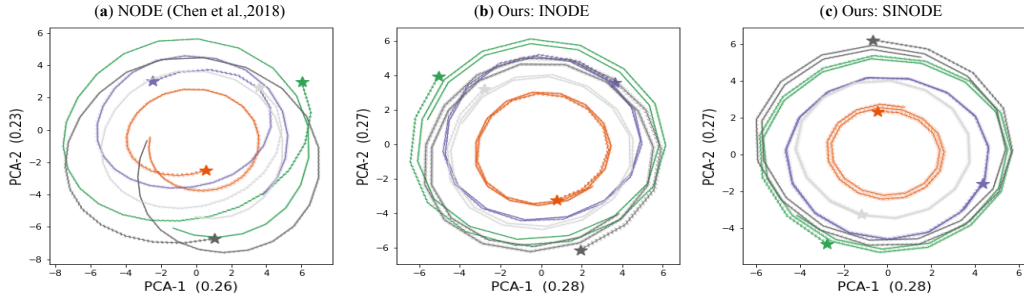


Figure 18. Sampled Rotating MNIST sequences latent space. (a) NODE [Chen et al. \(2018\)](#). (b) INODE(ours). (c) SIONDE (ours). A star indicates the beginning of a trajectory, while color indicates a data sample. In total six samples are plotted for $N_t=30$. Faint lines correspond to samples from the model, in total 50, while the thicker line is the mean value.

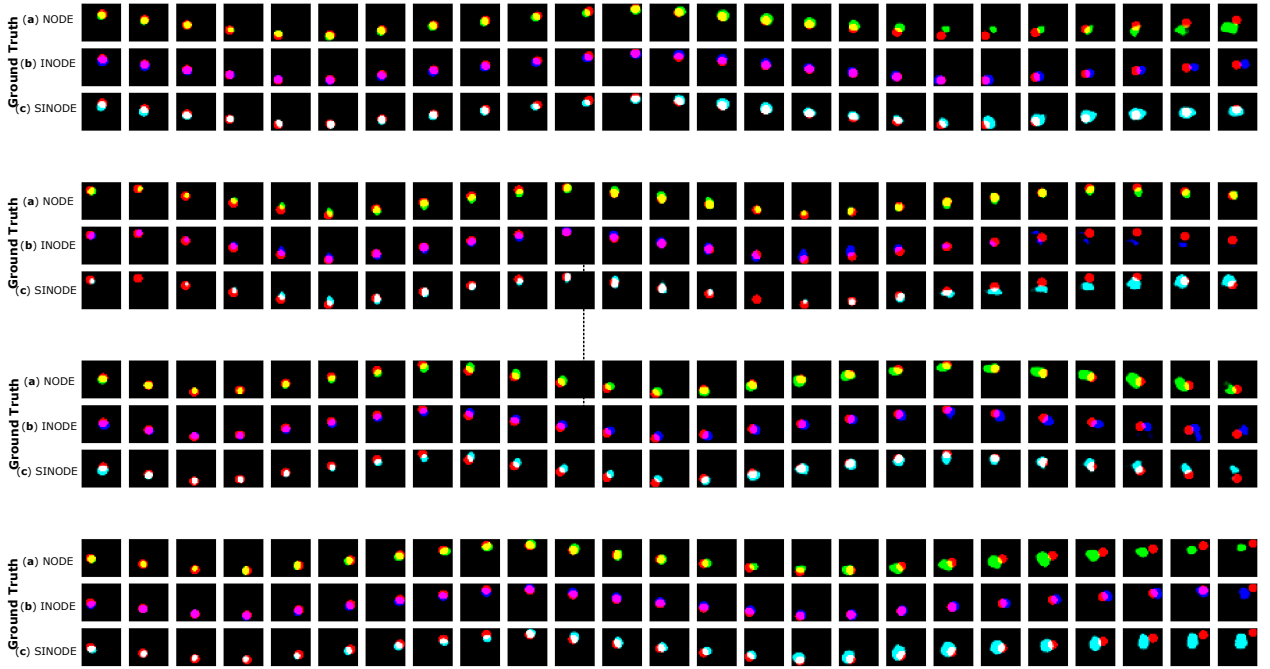


Figure 19. Bouncing ball test reconstructions for every even time frame. (a) NODE [Chen et al. \(2018\)](#) (b) INODE (ours). (c) SINODE (ours). The rows contrast the ground truth predictions (red) against the 3 models. At training time, NODE and INODE, SINODE condition on $T_{in} = 10$. Time-invariant content variable is learned from $T_{inv} = 10$ time frames. At test time, we roll out the model for a larger time interval ($N_t = 50$).